Robust Performance Analysis of Leader-Follower Systems Using Integral Quadratic Constraints

Tobias Augustin[1], Felix Biertümpfel[2], and Daniel Ossmann[1]

Abstract— **Leader-Follower systems play an essential role in modern robotics, yet achieving reliable formation control in the presence of model uncertainties and external disturbances remains a fundamental challenge. This paper presents a novel framework for analyzing the performance of leader-follower systems with respect to these effects over specific finite time horizons. Unknown communication delays between the agents, and dynamic uncertainties in the individual agents are considered as typical model uncertainties in leader-follower systems. Integral quadratic constraints are used to model the input/output behavior of these model uncertainties. This enables the application of dissipation arguments to pose an analysis condition for the worst-case performance. The resulting nonlinear optimization problem relies on solving parameterized Riccati differential equations. The approach is demonstrated on a leader-follower system composed of autonomous quadcopters under the aforementioned model uncertainties, as well as wind disturbance. The analysis shows a significantly faster analysis time compared to conventional Monte-Carlo simulation, while providing a guaranteed upper bound.**

I. INTRODUCTION

Over the past decade, the use of leader-follower systems has expanded across various fields, from commercial and environmental applications to disaster response. While individual agents have limited capabilities, deploying multiple agents cooperatively enables the efficient performance of complex tasks. Compared to single-vehicle operations, such leader-follower systems provide advantages in scalability, redundancy, and area coverage. Leader-Follower systems require, however, a form of control, e.g., controlling relative positions to each other. Formation control is a typical form of leader-follower control, where following agents hold a predefined position relative to their leader. It can either be centralized, i.e., the formation is controlled by a central control unit communicating with all agents, or decentralized. In decentralized control, every agent has its own controller to control its position within the formation, only requiring information from its adjacent agents. Especially in large formations, decentralized control is advantageous due to its reduced computational effort compared to its centralized counterpart, since computation is divided among the agents.

Decentralized leader-follower control is typically achieved using integrator backstepping [1], sliding mode- [2], optimal- [3] or PID-control [4]. To verify the safe operation of leader-follower systems, the closed-loop systems with their formation control algorithms need to be analyzed. Common methods determine the stability of these systems via methods of chain stability [5], [6]. These methods are limited to assessing the stability of the vehicle formation, offering only an indication of potential collisions. These methods do not analyze the leader-follower system with respect to uncertainties and specific disturbances, nor do they provide any specific performance metrics. While such verifications are commonly performed via Monte-Carlo simulations, they only provide a probabilistic measure, i.e., a lower bound, on the worst-case behavior and are computationally expensive.

Thus, this paper presents a novel approach to calculate an upper bound on the worst-case behavior of a leader-follower formation over a finite time horizon in the presence of uncertainties and external disturbances. The finite time horizon enables the analysis of the transient behavior of a leader-follower system. Because leader-follower systems often operate within specific tasks for a limited duration, this approach yields a less conservative bound on the worst-case gain compared to infinite time horizon analyses. The approach in this paper is based on the finite-horizon formulation of the bounded real lemma (BRL) [7]. Model uncertainties are expressed as integral quadratic constraints (IQCs). Firstly introduced in [8] for robustness analysis in the frequency domain, the IQC framework has been extended to the time domain [9], including periodic [10], linear parameter-varying [11], and linear time-varying [12], [13] systems in recent years. The BRL is solved in the present paper using the method introduced in [14]. This method is based on a nonlinear optimization constrained by the solvability of a parameterized Riccati differential equation (RDE), with details provided in Section II. Subsequently, Section III states a leader-follower control problem including model uncertainties in controlled leader-follower systems. These include time delays and dynamic model uncertainties as expressed as IQCs. The presented framework is demonstrated in Section IV for a formation of multicopter UAVs. In particular, the worst-case position in the presence of dynamic uncertainties, time delays, and wind disturbances of the follower relative to the leader is determined. The results are compared to Monte-Carlo simulations.

The paper contributes an efficient worst-case analysis ap-

This research is funded by the Bavarian State Ministry for Economic Affairs, Regional Development and Energy under the Air Mobility Funding Program BayLu25-III/HAMI, HAM-2307-0004.

[1]Tobias Augustin and Daniel Ossmann are with the Department of Mechanical, Automotive & Aeronautical Engineering, Munich University of Applied Sciences HM, Dachauer Strasse 98b, 80335 Munich, Germany. {tobias.augustin,daniel.ossmann}@hm.edu

[2]Felix Biertümpfel is with the Chair of Flight Mechanics and Control, TU Dresden, Marschner Str. 28, 01307 Dresden, Germany and the Department of Electrical and Computer Engineering, University of Michigan, 1301 Beal Avenue, Ann Arbor, MI 48109-2122, USA. felix.biertuempfel@tu-dresden.de,felixb@umich.edu

proach for leader-follower control problems. The calculated worst-case performance upper bounds the nonlinear system's behavior when compared to Monte-Carlo approaches using the nonlinear simulator. These bounds are also provided significantly faster, rendering the tool an efficient supplement to highly iterative control design and certification processes.

II. Finite Horizon LTI Robustness Analysis

Consider n interconnected, uncertain finite-horizon systems $\mathcal{P}_i := F_u(G_i, \Delta_i)$, $i = 1, ..., n$, as shown in Fig. 1, composed of the feedback interconnection of the known finite-horizon linear time-invariant (LTI) system G_i and uncertainty Δ_i. The interconnection $F_u(G_i, \Delta_i)$ is also known as the upper linear fractional transformation (LFT). The nominal system G_i is defined as

$$\begin{aligned} \dot{x}_{\mathcal{P}}^{(i)}(t) &= A^{(i)} x_{\mathcal{P}}^{(i)}(t) + B^{(i)} \begin{bmatrix} w^{(i)}(t) \\ d^{(i)}(t) \end{bmatrix} \\ \begin{bmatrix} v^{(i)}(t) \\ e^{(i)}(t) \end{bmatrix} &= C^{(i)} x_{\mathcal{P}}^{(i)}(t) + D^{(i)} \begin{bmatrix} w^{(i)}(t) \\ d^{(i)}(t) \end{bmatrix}. \end{aligned} \tag{1}$$

with state vector $x_{\mathcal{P}}^{(i)}(t) \in \mathbb{R}^{n_x^{(i)}}$, input vectors $d^{(i)}(t) \in \mathbb{R}^{n_d^{(i)}}$ and $w^{(i)}(t) \in \mathbb{R}^{n_w^{(i)}}$, and output vectors $e^{(i)}(t) \in \mathbb{R}^{n_e^{(i)}}$ and $v^{(i)}(t) \in \mathbb{R}^{n_v^{(i)}}$ at time $t \in [0, T]$, respectively. The state space matrices are real-valued and of adequate dimensions, e.g., $A^{(i)} \in \mathbb{R}^{n_x^{(i)} \times n_x^{(i)}}$. The uncertainty Δ_i, with $w^{(i)} = \Delta(v^{(i)})$, is defined by a causal operator $\Delta_i : L_{2[0,T]}^{n_v^{(i)}} \to L_{2[0,T]}^{n_w^{(i)}}$ with $v^{(i)} \in L_2[0, T]$, i.e., $\|v\|_{2[0,T]} = \left(\int_0^T v(t)^\intercal v(t) dt\right)^{0.5}$ is finite. To simplify notation, the superscript (i) will be omitted in the remainder of the paper whenever the association with a specific system is unambiguous. The interconnection $F_u(G_i, \Delta_i)$ is assumed to be well-posed as defined in Definition 1.

Definition 1: $F_u(G_i, \Delta_i)$ is well-posed if there exists unique solutions $x \in L_{2[0,T]}$, $v \in L_{2[0,T]}$, $e \in L_{2[0,T]}$ and $w \in L_{2[0,T]}$ satisfying (1) and $w = \Delta(v)$ for all $x(0) \in \mathbb{R}^{n_x}$ and $d \in L_{2[0,T]}$.

A. Integral Quadratic Constraints

In favor of readability, the following section describes the concept of finite horizon robustness analyses using IQCs for the interconnected uncertain system $\mathcal{P} = F_u(G, \Delta)$. In other words, the individual systems $\mathcal{P}_i$ are combined into the leader-follower system. For the finite horizon robustness analysis, the input-output behavior of the aforementioned model uncertainties is bounded with time-domain IQCs. A time-domain IQC is described by a stable LTI filter $\Psi \in \mathbb{RH}_\infty^{n_z \times (n_v + n_w)}$ and a symmetric matrix $M = M^\intercal \in \mathbb{R}^{n_z \times n_z}$. The filter's state vector is denoted as $x_\Psi \in \mathbb{R}^{n_{x_\Psi}}$, with inputs v and w and the output z. If the IQC

$$\int_0^T z(t)^\intercal M z(t) dt \geq 0 \tag{2}$$

is fulfilled for all $v \in L_2[0, T]$ and $w = \Delta(v)$ with zero initial conditions $x_\Psi(0) = 0$, the notation $\Delta \in \mathrm{IQC}(\Psi, M)$ is used. The IQC is only required to hold over a specific finite horizon $[0, T]$. This condition is closely related to so-called *hard* IQCs which have to hold over all finite time horizons $[0, \infty)$, see, e.g., [9]. Note that k model uncertainties $\Delta_k \in \mathrm{IQC}(\Psi_k, M_k)$ can be combined into a single IQC by diagonally combining the individual model uncertainties. The feedback interconnection of the nominal system G and the filter Ψ attached to the input and output of Δ can be seen in Fig. 2. The IQC can be incorporated into the worst-case analysis in three steps: 1) remove Δ, 2) treat w as external input, and 3) connect the signals v and w to the IQC filter Ψ and enforce the IQC (2) on the filter output z. The uncertainty output w is now implicitly bounded by the IQC. The extended state space system $\mathcal{P}_{\text{ext}}$, built by connecting $\mathcal{P}$ and Ψ is defined as

$$\begin{aligned} \dot{x}(t) &= \mathcal{A}x(t) + \begin{bmatrix} B_1 & B_2 \end{bmatrix} \begin{bmatrix} w(t) \\ d(t) \end{bmatrix} \\ \begin{bmatrix} z(t) \\ e(t) \end{bmatrix} &= \begin{bmatrix} C_1 \\ C_2 \end{bmatrix} x(t) + \begin{bmatrix} D_{11} & D_{12} \\ D_{21} & D_{22} \end{bmatrix} \begin{bmatrix} w(t) \\ d(t) \end{bmatrix}, \end{aligned} \tag{3}$$

where $x(t) = \begin{bmatrix} x_{\mathcal{P}}(t)^\intercal & x_\Psi(t)^\intercal \end{bmatrix}^\intercal \in \mathbb{R}^{n_{x_{\mathcal{P}}} + n_{x_\Psi}}$ contains the states of the nominal system G and the filter Ψ. Two time domain IQCs for typical model uncertainties in leader-follower problems are provided in Section III-B.

B. Finite Horizon Bounded Real Lemma

The worst-case performance of an uncertain LTI system over a finite time horizon interval $[0, T]$ can be quantified using the worst-case finite horizon L_2-to-Euclidean gain

$$\|F(G, \Delta)\|_2 := \sup_{\Delta \in \mathrm{IQC}(\Psi, M)} \sup_{\substack{d \in L_2[0,T] \\ d \neq 0,\, x_G(0) = 0}} \frac{\|e(T)\|_2}{\|d\|_{2[0,T]}}. \tag{4}$$

This gain can be interpreted as the ball upper bounding of the worst-case output of the interconnected system $\mathcal{P}_i$, $e(T)$, over all $\Delta \in \mathrm{IQC}(\Psi, M)$. To bound the worst-case gain (4) of the interconnection $F_u(G, \Delta)$, a dissipation inequality is formulated, using the extended system (3) and the IQC (2).

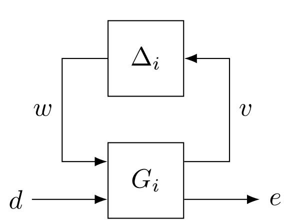

Fig. 1. Uncertain system $\mathcal{P}_i$.

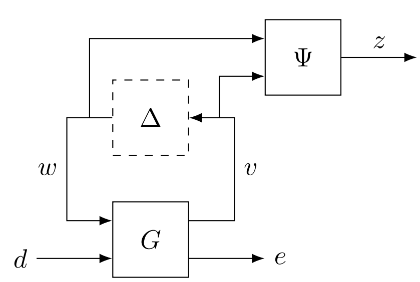

Fig. 2. Uncertainty Δ substituted with IQC filter.

This is described in [9] in detail. The analysis condition is given in Theorem 1.

Theorem 1: Let $F_u(G,\Delta)$ be well posed $\forall\Delta \in \mathrm{IQC}(\Psi, M)$. If there exists a continuously differentiable solution $P:\mathbb{R}_0^+ \to \mathbb{S}^{n_x}$ such that

$$P(T) = \frac{1}{\gamma} C_2^\intercal C_2 \tag{5}$$

$$\dot{P} = Q + P\tilde{A} + \tilde{A}^\intercal P - PSP \quad \forall t \in [0,T] \tag{6}$$

with

$$\tilde{A} = \begin{bmatrix} B_1 & B_2 \end{bmatrix} R^{-1} \begin{bmatrix} C_1^\intercal M D_{11}^\intercal \\ C_1^\intercal M D_{12}^\intercal \end{bmatrix} - \mathcal{A}, \tag{7}$$

$$S = -\begin{bmatrix} B_1 & B_2 \end{bmatrix} R^{-1} \begin{bmatrix} B_1^\intercal \\ B_2^\intercal \end{bmatrix}, \tag{8}$$

$$Q = -C_1^\intercal M C_1 + \begin{bmatrix} C_1^\intercal M D_{11}^\intercal \\ C_1^\intercal M D_{12}^\intercal \end{bmatrix}^\intercal R^{-1} \begin{bmatrix} C_1^\intercal M D_{11}^\intercal \\ C_1^\intercal M D_{12}^\intercal \end{bmatrix}, \tag{9}$$

and

$$R = \begin{bmatrix} D_{11}^\intercal M D_{11} & D_{11}^\intercal M D_{12} \\ D_{12}^\intercal M D_{11} & D_{12}^\intercal M D_{12} - \gamma^2 I \end{bmatrix} < 0, \tag{10}$$

then $\|F_u(G,\Delta)\|_2 < \gamma$.

Proof: The proof follows standard dissipation arguments and can be found in [12]. ■

C. Worst Case Gain Optimization

The condition in Theorem 1 has to be transferred into a computationally tractable problem. In general, an uncertainty can be described by an infinite number of IQCs. Thus, a common approach is to fix the IQC filter and optimize only over the IQC parameterization M confined to a set $\mathcal{M}$. This results in the nonlinear optimization problem

$$\begin{aligned} &\min_{M \in \mathcal{M}} \gamma \text{ s.t. } \forall t \in [0,T] \\ &P(T) = \frac{1}{\gamma} C_2^\intercal C_2 \\ &\dot{P} = Q + P\tilde{A} + \tilde{A}^\intercal P - PSP \\ &R < 0. \end{aligned} \tag{11}$$

This optimization problem is constrained by the solvability of the RDE (6) for a given M and γ. An efficient approach for solving (11) is presented in [14], which separates the optimization into an inner and outer loop. The inner-loop calculates the minimal feasible γ for a given M in a bisection over γ, while the outer-loop calculates an $M \in \mathcal{M}$. A nonlinear program is used to solve the outer loop problem and calculate a minimal γ. The optimization finishes once the desired accuracy is met. Note that for $\|d\|_{2[0,T]} = 1$ and $n_e = 1$, γ is a physically well-interpretable bound on the worst-case output value at the final time T.

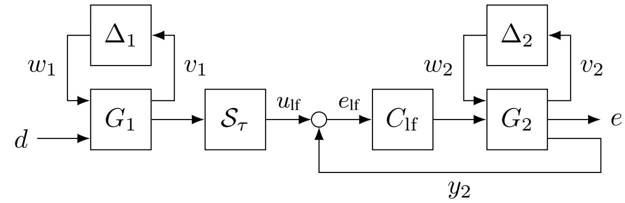

Fig. 3. Uncertain leader-follower controlled interconnection.

III. IQC Analysis of Leader-Follower Control

For simplicity, we assume two stable LTI systems G_i for $i \in \{1,2\}$ in a leader-follower relation, i.e., the system G_2 shall follow the leading system G_1 and hold a prescribed position relative to the leader. However, the approach directly extends to larger numbers of interconnected systems by notational changes. The goal is to keep the two controlled systems in formation by providing a defined point for G_2 relative to G_1. This point can be defined as a relative position or attitude of the follower with respect to the leader. A PID-like controller derived from [4], [15] is employed as a leader-follower algorithm. This is a typical multi-agent control approach where a (sub-)set of the outputs of the first system is relayed to the second system, for example, by means of data transmission. Figure 3 depicts the relation of the leader and follower systems. The two systems are connected via the leader-follower algorithm C_{lf}. Moreover, the combined system is subject to uncertainties, modeled via Δ_1 and Δ_2, arising from unmodeled dynamics and measurement uncertainties. Communication between the systems is subject to uncertain time delays $\mathcal{S}_\tau$. The next subsections introduce a leader-follower control algorithm C_{lf} followed by the modeling of the aforementioned typical model uncertainties encountered in multi-agent systems.

A. Leader-Follower Control

The algorithm only considers a planar movement of the systems, i.e., the systems can move along their body x- and y-axis and rotate around their z-axis. The i-th agent's rotation angle is denoted as θ_i, its position by $p_i = [p_{i,x}\, p_{i,y}]$. To ensure the follower is in a defined position behind the leader, first, the follower's deviation $\delta_E = [e_\tau \; e_v]^\intercal$ from the desired position behind the leader is calculated. This desired position, indicated in Fig. 4 as $(\oplus)$, is defined by the relative distance to the leader $\delta_{12}^{\mathrm{ref}}$ and the angle $\varphi_{12}^{\mathrm{ref}}$. The current distance δ_{12} is calculated by subtracting the followers position p_2 from the leader's position p_1, i.e., $\delta_{12} = |p_1 - p_2|$. The current angle between the leader and follower is calculated by

$$\varphi_{12} = \tan^{-1}\left(\frac{p_{1,y} - p_{2,y}}{p_{1,x} - p_{2,x}}\right). \tag{12}$$

This allows for the calculation of the deviation

$$e_\tau = \delta_{12}\cos\varphi_{12} - \delta_{12}^{\mathrm{ref}}\cos\varphi_{12}^{\mathrm{ref}} \tag{13}$$

in the global y-direction, and the deviation

$$e_v = \delta_{12}\sin\varphi_{12} - \delta_{12}^{\mathrm{ref}}\sin\varphi_{12}^{\mathrm{ref}} \tag{14}$$

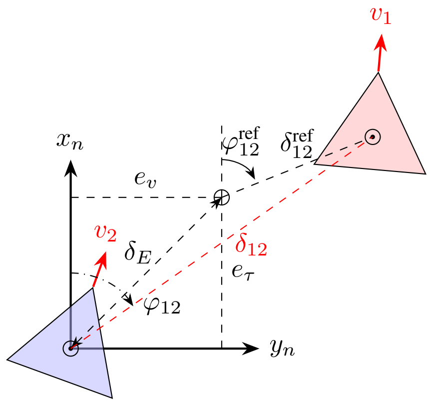

Fig. 4. Leader-Follower position error calculation.

in the global y-direction. These position errors are illustrated in Fig. 4, which also shows the agents' forward velocity v_i.

Given these position errors, we can define a control law that minimizes them and ensures that, once aligned, the follower matches the leader's forward velocity. This results in the control laws

$$v_2 = v_1 \frac{\cos(\beta_{12} - \varphi_{12}^{\mathrm{ref}})}{\varphi_{12}^{\mathrm{ref}}} + e_\tau K_v \tag{15}$$

and

$$\omega_2 = v_1 \frac{\sin \beta_{12}}{\delta_{12}^{\mathrm{ref}} \cos \varphi_{12}^{\mathrm{ref}}} + e_v K_\omega, \tag{16}$$

with $\beta_{12} = \theta_2 - \theta_1$, and K_v and K_ω being proportional controller gains for the linear and angular velocities.

The resulting formation controller C_{lf} has four inputs, i.e., the leader's positions $(p_{1,x},\, p_{1,y})$ and the leader's forward velocity v_1, all in its body-fixed reference frame, as well as the yaw angle θ_1. The controller outputs are the reference values for the follower system, i.e., references on forward velocity $v_{2,\mathrm{ref}}$ and yaw rate $\omega_{2,\mathrm{ref}}$.

B. Uncertainty Description of Multi-Agent Systems

Two main sources of model uncertainties are identified in the leader-follower interconnection. The first source of uncertainty is a communication delay $\mathcal{S}_\tau$ between the systems, more specifically, in the reference signal u_{lf} to the leader-follower control algorithm. Located between the output of G_1 and the controller C_{lf} as shown in Fig. 3, this delay can be caused by the time it takes to encode, transmit, and decode the data between the systems or by limited communication bandwidth. In small leader-follower systems with only a

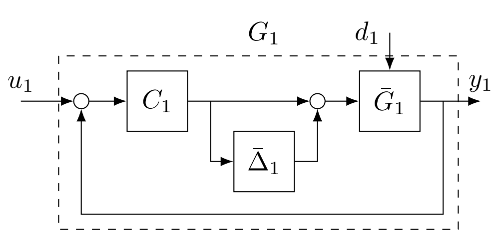

Fig. 5. Nominal system $\bar{G}_1$ extended with dynamic uncertainty and stabilizing controller.

few agents, the delay is primarily caused by the first factor. While real-world communication delays are time-varying, a standard modeling approach assumes a generalized worst-case value. Therefore, this analysis utilizes an uncertain fixed delay instead of a time-varying one [16]. Dynamic norm-bounded uncertainties in the dynamics of the individual agents are the second source of uncertainty. Fig. 5 shows the local closed loop, including the system $\bar{G}_1$, its dynamic model uncertainty $\bar{\Delta}_1$, and the local feedback controller C_1, leading to the stabilized system G_1. Therein, d_1 is the local disturbance acting on the system, u_1 the reference input, and y_1 the output position. With the system in LFT form, as shown in Fig. 2, the unknown bounded time delays and norm-bounded dynamic uncertainties can be approximated with the IQCs presented in the following two examples. [8]

Example 1: Dynamic Uncertainty Modeling via IQCs

Let $\Delta \in \mathbb{RH}_\infty$ and $\|\Delta\|_{[0,T]} \le b \in \mathbb{R}$ be a dynamic LTI uncertainty as shown in Fig. 2. A valid time-domain IQC(Ψ, M) is defined with $\Psi = \begin{bmatrix} D & 0 \\ 0 & D \end{bmatrix}$ and $M = \begin{bmatrix} b^2 & 0 \\ 0 & -1 \end{bmatrix}$. The filter D is a stable, minimum phase LTI system. A typical choice is

$$D = \begin{bmatrix} 1 & \dfrac{s+\rho}{s-\rho} & \cdots & \dfrac{(s+\rho)^a}{(s-\rho)^a} \end{bmatrix}^\intercal, \ \rho < 0,\, a \in \mathbb{N}_0. \tag{17}$$

Example 2: Time Delay Modeling via IQCs

Let Δ_τ be a bounded uncertain time delay $\tau \in \mathbb{R} > 0$. A valid time-delay is described by the conic combination of the two IQCs, IQC$_1(\Psi_{\tau_1}, \lambda_1 M_\tau)$ and IQC$_2(\Psi_{\tau_2}, \lambda_2 M_\tau)$, $\lambda_i > 0, i = 1, 2$. Ψ_{τ_1}, Ψ_{τ_2} and M_τ are the result of the J-spectral factorization [11] of the multipliers $\Pi_1 = \begin{bmatrix} 0 & -1 \\ -1 & 1 \end{bmatrix}$ and $\Pi_2 = \begin{bmatrix} 0 & \phi^*(s) \\ \phi(s) & -1 \end{bmatrix}$ as $\Pi_i = \Psi_{\tau_i}^\sim M_\tau \Psi_{\tau_i}$ with $\Psi\tau_i \in \mathbb{RH}_\infty^{n_z \times (m_1+m_2)}$ and $M_\tau = M_\tau^\intercal \in \mathbb{R}^{n_z \times n_z}$. A valid selection for $\phi(s)$ is

$$\phi(s) := \frac{-0.1072(\frac{s}{\tau})^3 - 1.346(\frac{s}{\tau})^2 - 272.8(\frac{s}{\tau}) - 5.849}{0.125(\frac{s}{\tau})^3 + 11.14(\frac{s}{\tau})^2 + 297.5(\frac{s}{\tau}) + 2182}, \tag{18}$$

as derived in [11].

Remark 1: The delay is defined with respect to the nominal signal. Time delay, therefore, requires a loop transformation shown in Fig 6. The bounded time-delay $\tilde{w} = \mathcal{D}_\tau(v) \in \mathbb{R}^{n_v}$ is defined by $\tilde{w} = v(t-\tau)$ with the time-delay $\tau \in [0, \tau_o]$ being a value between no time-delay and the delay margin τ_o. For robust stability analysis, it is more common to express the time-delay as the deviation between the delayed and the nominal signal, $\mathcal{S}_\tau := \mathcal{D}(v) - v$.

Integral quadratic constraints can thus describe the uncertainty set of the leader-follower system. This enables the application of the analysis condition in Theorem 1 and the formulation of the corresponding optimization problem.

IV. Application to UAV Formation Flight

Leader-follower control is a widely used strategy in leader-follower systems, particularly in the coordination of unmanned aerial vehicles (UAVs). Thus, we apply the performance analysis derived in the previous chapter to a simple multi-UAV system. Two UAVs shall fly in close formation, with the follower G_2 flying in a defined position behind the leading UAV G_1. The example considers a mission-specific task with a finite-time horizon of $T = 20\,\mathrm{s}$. To evaluate performance under model uncertainties and external disturbances, the worst-case deviation of the follower UAV from its nominal position over the time horizon is analyzed.

A. Multi-UAV System Model

Two quadcopter UAVs are considered in the study herein, which are supposed to move in formation, with the leader following a predefined trajectory. The nonlinear equations of motion are provided in [17] and are available as a MATLAB/Simulink implementation. The UAVs' inner-loop pitch- and roll-angle controllers are extended with an outer loop PID control scheme from [18], enabling velocity commands in the body-fixed frame. Additionally, yaw-rate and altitude of the UAVs are controlled, resulting in the reference input vector $u_{\text{ref}} = \left[v_{i,x}^{\text{ref}}\, v_{i,y}^{\text{ref}}\, \omega_i^{\text{ref}}\, h_i^{\text{ref}}\right]^\intercal$ for each drone.

The leader–follower algorithm follows the approach described in Section III-A. The controller gains are determined via loop-shaping using the nominal linearized model, and the controller parameters are manually tuned in the nonlinear simulation to achieve the desired controller behavior. The leader's forward velocity, yaw angle, and position are used to compute the follower's reference position and velocity. The reference point is defined by a desired separation distance of $d_{12}^{\text{ref}} = 2\,\mathrm{m}$ and an azimuth angle of $\varphi_{12}^{\text{ref}} = 45°$. Additionally, the leader's altitude is relayed to the follower as an altitude reference input, leading to a simple extension of the leader-follower structure into three dimensions, where the follower UAV vehicle holds the same altitude as the leader. Thus, the control algorithm C_{lf} has the inputs $u_{\text{lf}} = [p_1\, p_2\, \psi_1\, \psi_2\, v_{1,x}\, h_1]^\intercal$, and its outputs are the follower's reference altitude h_2^{ref}, yaw rate ω_2^{ref} and forward velocity $v_{2,x}^{\text{ref}}$ with $v_{2,y}^{\text{ref}} = 0$. The leader and follower UAVs are linearized independently, resulting in two linear models of the form (1). Straight and level forward flight with $v_{2,x}^{ref} = 10\ \mathrm{m/s}$ and $h = 30\ \mathrm{m}$ is chosen as the model trim-point for linearization. For the follower, the nonlinear leader–follower algorithm C_{lf} is incorporated before linearization and thus, also linearized. The individual linearization enables a straightforward inclusion of communication delays $\mathcal{S}_\tau$ between the models, when the two linearized UAV systems, i.e., the two UAVs G_1 and G_2, are interconnected as shown in Fig. 3. Therein, the interconnected system's performance output e is the follower's deviation δ_E from the reference formation point,

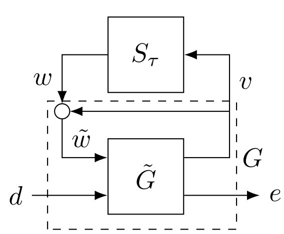

Fig. 6. Loop transformation for uncertain time-delays.

while the disturbance input d is an external wind force acting on the leader UAV. This input and the considered model uncertainties Δ_1 and Δ_2 are discussed in more detail next.

1) Disturbance Input: The disturbance input d represents a wind disturbance acting on the leader UAV's x- and y-axis, which in turn induces an external force F_d on the UAV in these directions. In the robustness analysis, the disturbance input remains norm-bounded such that $\|d\|_{2[0,T]} \leq 1$, thereby covering any admissible disturbance signal within these bounds. Accordingly, in the nonlinear simulation, this disturbance is modeled as a norm-bounded step input, where the gust duration is treated as a free parameter, and the gust amplitude is adjusted to ensure that $\|d\|_{2[0,T]} \leq 1$ is satisfied.

2) Model Uncertainties: Norm-bounded dynamic LTI uncertainties are used to describe the model uncertainties. The norm bound quantifies a relative modeling error, e.g., a norm bound of 0.2 describes a $20\,\%$ model uncertainty. While specific parameters like vehicle mass are generally well known, the dynamic uncertainty represents unknown vehicle dynamics such as unmodeled structural dynamics. Time delays are represented as input delays of the form $e^{-\tau s}$, with a maximum delay of $\tau_o = 0.5\,\mathrm{s}$. A time-domain IQC derived from (18) is used. Accordingly, in the nonlinear simulation, the dynamic model uncertainties are represented using MATLAB's `ultidyn` function, where for every simulation a random LTI model with a norm-bound of 0.2 is sampled. The uncertain time delays are implemented using Simulink's transport delay block. For each simulation, a time delay between $0\,\mathrm{s}$ and $0.5\,\mathrm{s}$ is sampled.

B. Robustness Analysis

For the finite time-horizon robust performance analysis, the model uncertainties are substituted by IQCs. Therefore, the uncertain multi-UAV system is brought into LFT form, i.e., separating the uncertainties from the interconnected LTI system. Subsequently, the uncertainties, described in Section IV-A are replaced by the corresponding IQC filters.

The analysis is performed by solving the optimization problem (11) using the open-source MATLAB toolbox OPTI [19]. In particular, the derivative-free, nonlinear optimizer Constrained Optimization BY Linear Approximation (COBYLA), described in [20], [21], is used. The algorithm performs the following steps in every iteration i: First, it is checked whether a solution to the RDE exists for the given M using the current upper bound γ_{ub}. If a solution is found, the bisection is performed to minimize γ_i. Therein, the RDE is solved with MATLAB's backward integration algorithm `ode15s`. If the RDE is infeasible, γ_i is set to the initial value of γ_{ub}, and the optimization continues with a different M determined by the optimizer. If the RDE is solvable and the bisection yields a value $\gamma_i < \gamma_{\text{ub}}$, the upper bound γ_{ub} is updated to this new γ_i for the next iteration over M. Finally, if the accuracy $|\gamma_{i-1} - \gamma_i| < \epsilon_{\text{opt}}$ is met, the overall optimization stops. For the multi-UAV system, the worst-case performance analysis yields an upper bound of $0.205\,\mathrm{m}$, representing the maximum deviation from the nominal trajectory deviation δ_E at the end of the time

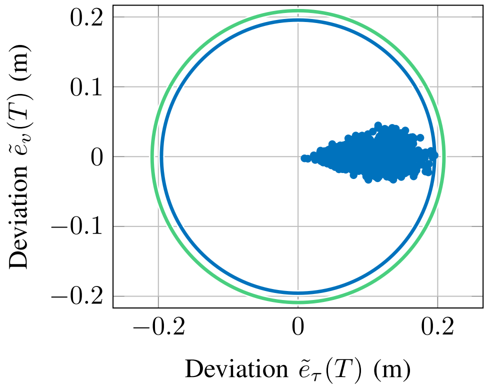

Fig. 7. Deviations in x- and y-direction of the follower UAV from its nominal position at $t = T$, including the bounds computed with the IQC-based approach (—) and a Monte-Carlo simulation (—).

horizon of $20\,s$. The analysis is performed in MATLAB 2024b on a customer PC with an AMD Ryzen 7 1700X 3.4 GHz Eight Core Processor with 16 GB of RAM, with an overall runtime of 1338 s. To verify the calculated upper bound, a Monte-Carlo analysis is performed on the full nonlinear simulator with the described disturbance inputs and uncertainties in Section IV-A. A total of 8000 simulations are performed, requiring an overall simulation time of 5053 s, which is nearly a factor of four longer than the worst-case performance analysis. The Monte-Carlo analysis results in a lower bound of $0.195\,\mathrm{m}$. These results confirm that the computed upper bound with the approach presented herein is not overly conservative and requires much less computational effort to be derived. For visualization of the results, Fig. 7 illustrates the deviations $\tilde{e}_\tau$ and $\tilde{e}_v$ from the nominal position errors e_τ and e_v projected in earth coordinates. The upper bound on $\tilde{\delta}_E$, found by the worst case performance analysis, is indicated by (—). Also depicted is the resulting lower bound gained through the Monte-Carlo simulations (—), bounding the Monte-Carlo runs, indicated by the blue dots. The figure confirms a satisfactory quality of the computed upper bound. Note that the proposed method efficiently computes the depicted bound at the end of the time horizon. To confirm that the worst-case computation at the end of the time horizon is adequate for the given example, Fig. 8 illustrates the deviation $\tilde{\delta}_E$ obtained from the Monte Carlo analysis over the whole considered time horizon of 20 s. The computed upper bound (—) is not exceeded at any point in time, finally confirming its overall validity.

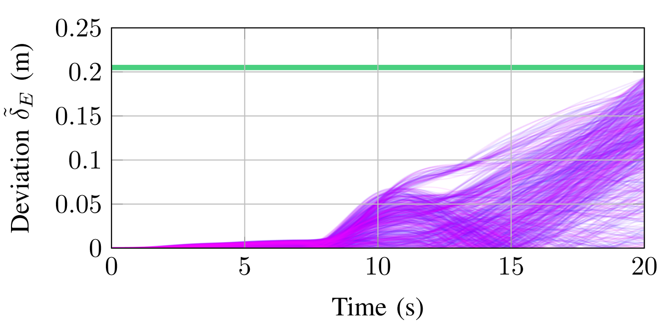

Fig. 8. Deviation $\tilde{\delta}_E$ from nominal follower position over the time horizon for 8000 simulation runs and the computed upper bound (—).

V. Conclusion

A method for quantifying the robust performance of leader-follower systems by evaluating the upper bound of the finite-horizon induced L_2-to-Euclidean gain is presented. The method indicates clear advantages over Monte-Carlo analyses, including reduced computation times and guaranteed worst-case behavior. The results highlight the method's effectiveness as an adaptable and efficient tool for assessing the robustness and performance of leader-follower systems. Future work will address scalability and sensitivity of the approach.

References

[1] X. Li, J. Xiao, and Z. Cai, "Backstepping based multiple mobile robots formation control," in *2005 IEEE IROS*, Aug. 2005.

[2] M. Defoort, T. Floquet, A. Kokosy, and W. Perruquetti, "Sliding-Mode Formation Control for Cooperative Autonomous Mobile Robots," *IEEE Trans. Ind. Electron.*, vol. 55, no. 11, 2008.

[3] Y. Zhou, X. Dong, G. Lu, and Y. Zhong, "Time-varying formation control for unmanned aerial vehicles with switching interaction topologies," in *2014 ICUAS*, 2014.

[4] I.-S. Choi and J.-S. Choi, "Leader-Follower Formation Control Using PID Controller," *2012 ICIRA*, 2012.

[5] J. R. Riehl, E. A. L. Hufstedler, P. Chatelain, and J. M. Hendrickx, "String Stability of Energy-Saving Aircraft Formations," *J. Guid. Control Dyn.*, vol. 45, no. 5, 2022.

[6] P. Seiler, A. Pant, and K. Hedrick, "Disturbance propagation in large interconnected systems," *American Control Conference*, 2002.

[7] M. Green and D. J. N. Limebeer, *Linear Robust Control*. USA: Prentice-Hall, Inc., 1994.

[8] A. Megretski and A. Rantzer, "System analysis via integral quadratic constraints," *IEEE Trans. Autom. Control*, vol. 42, no. 6, 1997.

[9] P. Seiler, "Stability Analysis With Dissipation Inequalities and Integral Quadratic Constraints," *IEEE Trans. Autom. Control*, vol. 60, no. 6, 2015.

[10] D. Ossmann and H. Pfifer, "Robustness analysis of continuous periodic systems using integral quadratic constraints," *IEEE 58th CDC*, 2019.

[11] H. Pfifer and P. Seiler, "Integral quadratic constraints for delayed nonlinear and parameter-varying systems," *Automatica*, vol. 56, 2015.

[12] P. Seiler, R. M. Moore, C. Meissen, M. Arcak, and A. Packard, "Finite horizon robustness analysis of LTV systems using integral quadratic constraints," *Automatica*, vol. 100, 2019.

[13] F. Biertümpfel, N. Pholdee, S. Bennani, and H. Pfifer, "Finite horizon worst case analysis of linear time-varying systems applied to launch vehicle," *IEEE Trans. Control Syst. Technol.*, vol. 31, no. 6, 2023.

[14] F. Biertümpfel and H. Pfifer, "Worst Case Gain Computation of Linear Time-Varying Systems over a Finite Horizon," *2018 IEEE CCTA*, 2018.

[15] L. Consolini, F. Morbidi, D. Prattichizzo, and M. Tosques, "Leader–follower formation control of nonholonomic mobile robots with input constraints," *Automatica*, vol. 44, no. 5, 2008.

[16] X. Liu, L. Dou, and J. Sun, "Consensus for networked multi-agent systems with unknown communication delays," *Journal of the Franklin Institute*, vol. 353, no. 16, 2016.

[17] D. Mellinger, N. Michael, and V. Kumar, "Trajectory generation and control for precise aggressive maneuvers with quadrotors," *The Int. J. of Robotics Research*, vol. 31, no. 5, 2012.

[18] T. Augustin and D. Ossmann, "Multi-Mode Control enabling optimized Unmanned Aerial Vehicle Firefighting Performance," *AIAA Scitech Forum*, 2025.

[19] J. Currie and D. I. Wilson, "OPTI: Lowering the barrier between open source optimizers and the industrial MATLAB user," in *Foundations of Computer-Aided Process Operations*, Savannah, GA, USA, 2012.

[20] M. J. Powell, "A direct search optimization method that models the objective and constraint functions by linear interpolation," in *Advances in optimization and numerical analysis*. Springer, 1994.

[21] ——, "Direct search algorithms for optimization calculations," *Acta Numerica*, vol. 7, 1998.